Reaction Chemistry & Engineering

ROYAL SOCIETY OF CHEMISTRY

PAPER

View Article Online
View Journal | View Issue

Cite this: *React. Chem. Eng.*, 2023, **8**, 1943

Integrated low carbon H_2 conversion with *in situ* carbon mineralization from aqueous biomass oxygenate precursors by tuning reactive multiphase chemical interactions†

Prince Ochonma, [a] Christopher Noe,[b] Sohaib Mohammed, [c] Akanksh Mamidala[c] and Greeshma Gadikota *[ac]

Meeting our rising demand for clean energy carriers such as H_2 from renewable biomass resources is challenged by the co-emission of CO_2 and CH_4. To address this challenge, we design novel reactive separation pathways that integrate multiphase chemical reactions by harnessing Ca and Mg bearing minerals as a sorbent to capture CO_2 released during the hydrothermal deconstruction of aqueous biomass oxygenates to produce H_2 and solid carbonates *via* low temperature aqueous phase reforming and thermodynamically downhill carbon mineralization. Earth abundant catalysts such as Ni/Al_2O_3 are effective in producing H_2 yields as high as 79% and 74% using ethylene glycol and methanol in the presence of $Ca(OH)_2$ as an alkaline sorbent, without contaminating or deactivating the catalyst. H_2 yields with *in situ* carbon mineralization using a Ni or Pt/Al_2O_3 catalyst are enhanced based on the following order of reactivity: acetate < glycerol < methanol < formate < ethylene glycol. These studies demonstrate that the multiphase chemical interactions can be successfully tuned to enhance H_2 yields through the selective cleavage of C–C bonds using Ni/Al_2O_3 catalysts to deconstruct biomass oxygenates for producing H_2 and CO_2, and *in situ* carbon mineralization by harnessing abundant alkaline materials, as demonstrated using ladle slag. This approach unlocks new scientific possibilities for harnessing multiple emissions including abundant organic-rich wastewater streams and alkaline industrial residues to co-produce low carbon H_2 and carbonate-bearing materials for use in construction by using renewable solar thermal energy resources.

Received 12th December 2022,
Accepted 24th March 2023

DOI: 10.1039/d2re00542e

rsc.li/reaction-engineering

1. Introduction

Advancing sustainable low carbon chemical pathways for meeting our energy needs while limiting detrimental impacts on climate and the environment is our societal and scientific grand challenge.[1] One emerging approach to realize rapid decarbonization is by harnessing hydrogen as a sustainable and clean energy carrier[2,3] for use in industrial processes, fuel cells, transportation, and heating. Hydrogen generated with inherent carbon removal and *via* electrolysis of water resources has the potential to decarbonize sectors which pose a challenge to abating CO_2 emissions such as aviation, long distance transportation, and shipping which contributes ~2.2 Gt to annual CO_2 emissions.[1] Current methods for producing hydrogen at commercial scales require energy-intensive, high-temperature steam methane reforming (SMR) of non-renewable feedstocks which results in significant CO_2 emissions.[4] SMR for H_2 production contributes about 3% to the global CO_2 emissions annually (~1.2 Gt of CO_2 per year).[5] Despite the promise of H_2 generation *via* water electrolysis (also known as green electrolysis), significant scientific and technological advances are needed to achieve favorable economics for scalable deployment.[6]

One of the less explored but highly promising approaches is to harness low value and renewable aqueous biomass oxygenates such as bio-derived methanol, ethylene glycol, ethanol, formate and acetate for producing H_2.[4,7–9] Depending on the sourcing and processing conditions, the use of aqueous bio-derived feedstocks for H_2 production has the potential to be carbon neutral.[10] Bio-derived oxygenates are abundant in wastewater from biomass processing. For

[a] *Robert Frederick Smith School of Chemical and Biomolecular Engineering, Cornell University, 113 Ho Plaza, Ithaca, NY 14853, USA. E-mail: gg464@cornell.edu; Tel: +1 607 255 4796*
[b] *Department of Chemistry, College of Art and Science, Stony Brook University, Stony Brook, NY 11790, USA*
[c] *School of Civil and Environmental Engineering, Cornell University, 527 College Avenue, 117 Hollister Hall, Ithaca, NY 14853, USA*
† Electronic supplementary information (ESI) available. See DOI: https://doi.org/10.1039/d2re00542e

instance, bio-methanol, glycerol, and ethylene glycol are major by-products of bio-based fuel processing.[11,12] In 2020, about 1817 million gallons of biodiesel was produced in the United States.[13] Every gallon of biodiesel produced generates approximately 1.05 pounds of glycerol.[14] Formate and acetate are produced in massive quantities from the anaerobic digestion of food waste and wastewater sludge.[15,16] Upcycling aqueous biomass oxygenates to produce H_2 is a less conventional but unique approach that valorizes these waste streams and enhances resource utilization as opposed to treating them as a waste in need of remediation.

Approaches to produce H_2 from aqueous biomass oxygenates at 200–300 °C in pressurized N_2 environments in the presence of a metal catalyst[8,17] have resulted in high H_2 yields. However, in this process, which is also known as aqueous phase reforming (APR), H_2 evolution is accompanied by the co-generation of CO_2. One scientific challenge in APR lies in enabling the cleavage of C–C bonds to promote H_2 and CO_2 evolution as opposed to C–O bond cleavage which results in CH_4 formation. This challenge has been resolved by using catalysts such as Ni and Pt which have been shown to favor the cleavage of C–C bonds.[8,17] One of the key advantages of this approach is that the water content co-present with biomass oxygenates can be synergistically harnessed for H_2 conversion. Potentially limiting reaction kinetics and thermodynamics due to elevated pressures and hydrothermal conditions are overcome by harnessing catalysts to selectively cleave biomass oxygenate molecules. In contrast to conventional biomass gasification which occurs at temperatures >500 °C,[18] this approach harnesses significantly lower temperatures in the range of 200–250 °C, which can be achieved using renewable solar thermal energy resources.[19]

To date, research conducted on enhancing H_2 yields from aqueous biomass oxygenates has focused on the role of catalysts in enhancing reactivity. For example, Vaidya and Lopez-Sanchez[8] summarized the influence of group VIII metal catalysts such as Ni and Pt on metal oxide supports (*e.g.*, Al_2O_3) in aiding the C–C cleavage of biomass oxygenate molecules to produce H_2 and CO_2.

Extensive studies have been conducted on harnessing biomass oxygenates such as glycerol,[20] sorbitol,[21] xylitol,[22] methanol,[17] ethanol,[23] acetic acid,[24] and butanol.[25] Conversions of 10–60 wt% aqueous feed concentrations of glucose,[21] cellulose,[26] and glycols[27] have been reported, demonstrating that this process is also effective for converting non-volatile biomass feedstocks into H_2. Despite the promise of aqueous phase reforming, achieving high H_2 selectivity remains a challenge. The competing methanation reaction which involves the reaction of H_2 and CO/CO_2 (ref. 8) to produce CH_4 limits the H_2 yield and selectivity. Slower kinetics at lower temperatures in the range of 200–250 °C as opposed to temperatures greater than 500 °C may limit H_2 yields due to the endothermic nature of biomass deconstruction pathways.[28] In addition to H_2 selectivity and kinetic limitations, significant quantities of CO_2 are co-produced, which implies that an additional unit for separation and purification of gas streams is essential to produce low carbon H_2. Thus, novel chemical pathways need to be designed for highly selective, energy- and atom-efficient reactive separation of CO_2 integrated with H_2 conversions from aqueous biomass oxygenate precursors.

Several approaches exist for CO_2 capture and removal post energy and resource conversion processes. CO_2 capture involves separating CO_2 in dilute flue gas streams to produce a CO_2-rich stream and CO_2-lean stream using adsorbents, absorbents, and membranes.[29–31] Furthermore, approaches to remove CO_2 *via* carbon mineralization obtained post CO_2 capture have been investigated. Carbon mineralization is a thermodynamically downhill pathway for converting gaseous CO_2 into solid carbonates. Specifically, pH swing approaches, in which acids are used to facilitate the dissolution of alkali-bearing minerals and residues followed by bases to enhance carbonate concentrations for solid carbonate formation, have been well established.[32] As an alternative to these carbon mineralization pathways, single step approaches in which regenerable solvents are used to enhance CO_2 capture and mineralization to produce solid carbonates, which results in the chemical regeneration of the solvents,[30,33,34] have been shown to be very effective without the need for external reagents for pH swing.

While post combustion CO_2 capture and mineralization has been shown to be effective, the integration of H_2 conversion with CO_2 mineralization remains less explored. Coupling thermodynamically downhill carbon mineralization pathways with uphill energy and resource conversions has the net impact of lowering the overall energy needs while contributing to inherent carbon removal. For example, coupling the water gas shift reaction with carbon mineralization of Ca- and Mg-silicates is favored at elevated temperatures in the range of 150–250 °C and pressurized gaseous environments.[35] This approach is inspired by evidence of more than an 80% conversion of olivine ($(Mg, Fe)_2SiO_4$) to magnesium carbonate at elevated partial pressures of CO_2 in the range of 100–150 atm and temperatures in the range of 150–185 °C.[36] Enhanced H_2 yields with inherent carbon removal *via* mineralization remains less explored in the context of using aqueous biomass oxygenates. The conditions that favor carbon mineralization including elevated temperatures, high CO_2 partial pressures and aqueous slurry environments are well-aligned with the deconstruction of biomass oxygenates to produce H_2 with inherent removal of CO_2. Elevated temperatures increase the reactivities of Ca- and Mg-oxides, hydroxides, and silicates[37] and enhance the precipitation of solid Ca- and Mg-carbonates whose solubility decreases with increasing temperature[38] The high pressure at which these reactions proceed also implies enhanced CO_2 capture rates, due to increased CO_2 solubility.[39]

In a prior study, we showed that suppression of methane formation using catalysts and the presence of alkaline resources (*e.g.*, calcium oxide) to capture CO_2 are effective in

enhancing H_2 yields from bio-derived aqueous feedstocks such as ethanol, methanol, glycerol, ethylene glycol, acetone, and acetic acid.[28] The reaction representing enhanced H_2 yield with inherent carbon removal is as follows:

$$C_xH_yO_z + xCaO + (2x–z)H_2O \rightarrow xCaCO_3 + (2x–z + 0.5y)H_2 \quad (R1)$$

The proposed *in situ* CO_2 capture approach from aqueous biomass oxygenate resources does not require expensive separation of CO_2, utilizes enormous quantities of available feedstocks, and can be integrated into existing biorefineries. A key consideration is the suppression of methane evolution using a catalyst such as Pt or Ni. Platinum supported on alumina has been shown to result in high yield and selectivity to H_2.[27] As an alternative to catalysts synthesized from precious metals, nickel-bearing catalysts have been proposed as an economical alternative. Low H_2 selectivity in the presence of Ni-based catalysts[17] motivated research efforts to dope these catalysts with Cu, Ce and Sn and use various metal oxides and carbonaceous materials as supports to enhance H_2 selectivity.[40–42]

Prior work showing the thermodynamic feasibility of enhancing H_2 yields with inherent carbon removal from aqueous biomass oxygenates using calcium oxide has opened new possibilities for harnessing alkaline industrial residues bearing calcium oxide. Among alkaline industrial residues, ladle slag (LS) generated as a by-product of post-processing molten steel produced from the EAF steel making process has significant potential to store CO_2 due to its high calcium and magnesium content.[43] However, large quantities of these residues still end up in landfills with significant disposal costs and detrimental environmental impacts. The valorization potential of these materials is low due to their weak cementitious properties, low strength, and potential leaching of heavy metals which can inhibit utilization for several key applications.[44] Accelerated carbon mineralization of ladle slag can upgrade their chemical and mechanical properties which is beneficial to subsequent utilization as construction materials in blended cement or concrete.[44,45] Incorporating compositions as low as 10 wt% of carbonate-bearing steel slag in construction materials has been shown to enhance the compressive strength from about 33–50 MPa.[33] Recent studies have reported that the heavy metal immobilization potential can also be enhanced by carbon mineralization.[44,46] The direct use of alkaline industrial residues rich in Ca- or Mg-oxides and hydroxides circumvents the need to produce high purity Ca- or Mg-oxides and hydroxides for carbon mineralization. The proposed approach contributes to the upcycling of multiple low-value streams including aqueous biomass oxygenates and ladle slag to produce H_2 with inherent carbon removal and can establish a waste-to-resource supply chain for advancing a low carbon H_2 economy, as shown in Fig. 1.

Despite the promising potential of these pathways to produce H_2 with inherent carbon removal, several open scientific challenges remain. First, the kinetics and

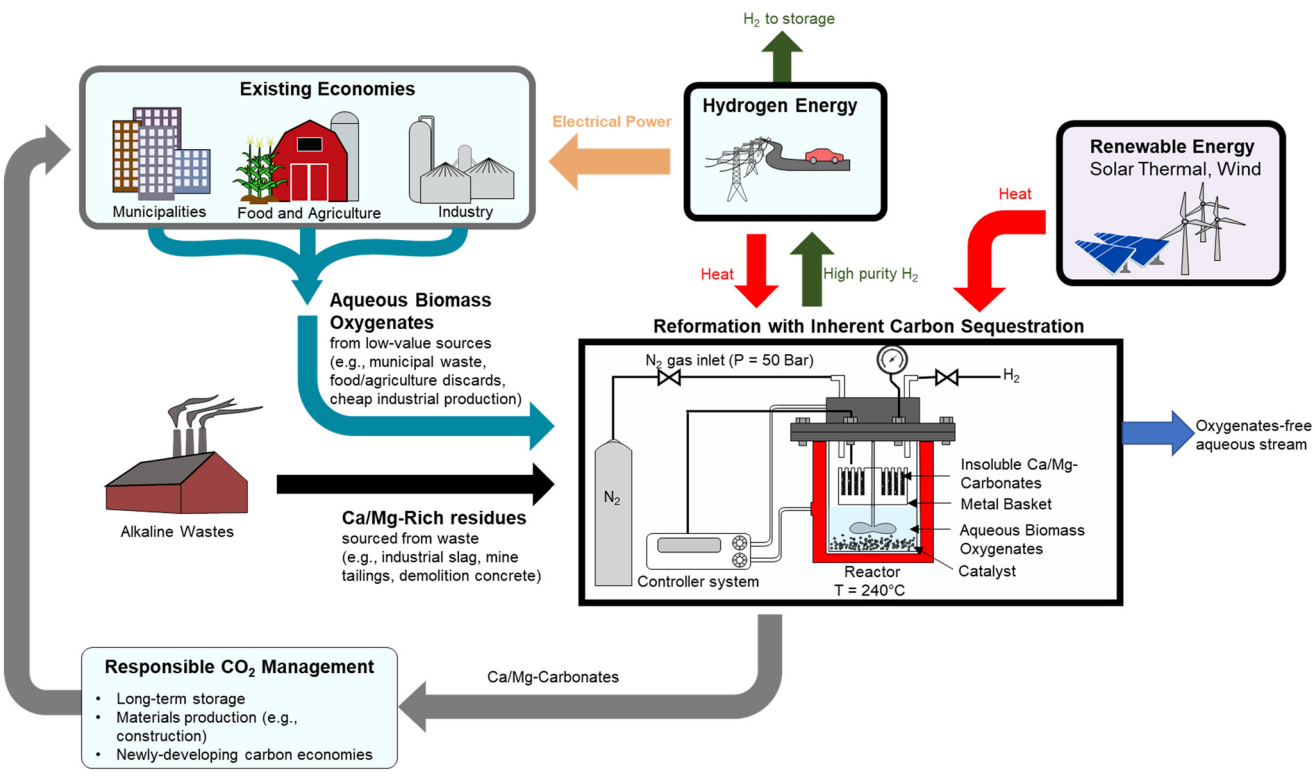

Fig. 1 Schematic representation of integrated H_2 production from aqueous biomass oxygenates with *in situ* CO_2 capture using alkaline industrial residues.

mechanisms associated with enhanced H_2 recovery with inherent carbon removal from biomass oxygenates remain unresolved. Second, the hypothesis, in which nickel-bearing catalysts can be effective in enhancing H_2 yields with inherent carbon removal as an alternative to platinum-bearing catalysts, has not been investigated. Third, the effectiveness of various reaction modes in enhancing H_2 yield and selectivity, such as those in which the alkaline residues, catalysts and oxygenates are co-present in the aqueous phase (referred to as mode I in this study) *versus* placing the alkaline residue in the gas phase while the biomass oxygenates and catalysts are in the aqueous phase (referred to as mode II in this study), has not been studied. Fourth, the enhancement in H_2 yield and selectivity associated with using alkaline industrial residues such as ladle slag has not been contrasted with that of pure calcium hydroxide. Fifth, the mechanisms associated with the deconstruction of biomass oxygenates and associated reactivity based on their structure have not been elucidated. Sixth, identification of the rate limiting step in multiphase chemical transformations is not trivial. In the context of enhanced H_2 recovery with inherent carbon removal, biomass deconstruction, selective H_2 formation over CH_4 evolution, CO_2 solubility, or the conversion of CO_2 to solid carbonate could be rate limiting. Identifying the rate limiting step is crucial for developing approaches to accelerate low carbon H_2 recovery. Therefore, the aim of this study is to elucidate the mechanisms and rates of enhanced H_2 production with inherent carbon removal from aqueous biomass oxygenates such as methanol, ethylene glycol, acetate, formate, and glycerol using calcium hydroxide as an alkaline sorbent. The effectiveness of using ladle slag for *in situ* carbon capture is investigated.

The proposed approach of harnessing low value aqueous biomass oxygenates for enhanced H_2 yield with inherent carbon removal is transformative. This approach adds to the portfolio of technologies for bioenergy with carbon capture and storage (BECCS) which involves harnessing bioenergy while capturing and storing biogenic CO_2.[47] In 2018, the IPCC reported that BECCS can contribute to carbon offsets on the order of ~0.5–5 Gt CO_2 per year with costs in the range of $100–200 per ton of CO_2.[48] These estimates were based on conventional BECCS technologies where biomass is co-fired with coal in a power plant and the captured CO_2 is stored in a subsurface geologic environment. The proposed approach of producing H_2 with inherent carbon removal from aqueous biomass oxygenates eliminates the need for *in situ* CO_2 storage and monitoring over long periods of time. Advances in solar thermal energy technologies facilitate the distributed conversion of aqueous biomass oxygenates to H_2 with inherent carbon removal. Fundamental mechanistic insights into the deconstruction of aqueous biomass oxygenates to produce low carbon H_2 developed through this study are crucial for the scalable realization of these pathways for implementation.

2. Materials and methods

2.1 Materials

High purity oxygenates such as methanol (99.9%, Thermo Fisher Scientific), glycerol (99.5%, Thermo Fisher Scientific), ethylene glycol (99.7%, Thermo Fisher Scientific), sodium acetate (99%, Fisher Bioreagents), and sodium formate (99.9% Acros Organics) were used as model wastewater bio-oxygenates in this study. Platinum (Pt) and nickel (Ni) on an alumina (Al_2O_3) support were used as catalysts in these experiments. A Pt/Al_2O_3 catalyst with a composition of 5 wt% was obtained from Sigma Aldrich. A Ni/Al_2O_3 catalyst with a composition of 5 wt% was synthesized in the lab *via* the incipient wetness impregnation method. To synthesize the Ni/Al_2O_3 catalyst, γ-Al_2O_3 (Strem Chemicals Inc., 97%) was impregnated with a solution bearing $Ni(NO_3)_2{\cdot}6H_2O$ (Thermo Fisher Scientific). Post impregnation, the samples were dried at 80 °C, calcined at 450 °C (±5 °C) for 3 hours, and then reduced in a flowing N_2 : H_2 (95% : 5%) gas mixture at 450 °C (±5 °C) for 5 hours. Calcium hydroxide (Thermo Fisher Scientific), and ladle slag (LD) from Nucor's electric arc furnace (EAF) steel making plant in Auburn, NY were used as the alkaline sorbents for this study.

Elemental analysis of ladle slag. The major constituent compositions of ladle slag used as an alkaline sorbent in this study were determined using wavelength dispersion X-ray fluorescence (WD-XRF, Panalytical Axios) as shown in Table 1. Prior to elemental analyses, the samples were crushed and pulverized followed by the formation of a homogeneous glass disk by the fusion of the sample and a lithium tetraborate/lithium metaborate mixture. The loss on ignition (LOI) was determined separately and gravimetrically at 1000 °C. The prepared disks were analyzed by wavelength dispersion X-ray fluorescence (WD-XRF). The LOI was included in the matrix correction calculations, which were performed by the XRF software. X-ray photoelectron spectroscopy (XPS, Scienta Omicron ESCA-2SR, Al Kα) surface analysis and inductively coupled plasma optical emission spectrometry were utilized to confirm the weight ratio of the

Table 1 Major elemental compositions of ladle slag (wt%) using X-ray fluorescence analyses (XRF). The ladle slag is a by-product of Nucor's electric arc furnace steel making process

Compositions (%)	Nucor electric arc furnace ladle slag
SiO_2	9.66
Al_2O_3	11.20
Fe_2O_3	5.35
MgO	31.30
CaO	33.40
Na_2O	0.08
K_2O	0.10
TiO_2	0.51
P_2O_5	0.09
MnO	0.92
Cr_2O_3	0.11
V_2O_5	0.02
LOI	6.40
C (t)	0.34
S	0.14

Ni and Pt metals to the Al_2O_3 support used in this study as shown in Fig. S1.†

Determination of the chemical composition of the solid samples. The thermal behavior of the alkaline sorbents and their reacted products were determined using a thermogravimetric analyzer (TGA, Discovery SDT 650, TA Instrument), and total carbon analysis (TCA, LECO CS 844). In a typical TGA run, samples were exposed to a N_2 environment (flow rate: 50 ml min^{-1}) as the temperature was ramped from 25 °C to 1000 °C at a rate of 10 °C min^{-1}. Based on the weight drop related to each dehydroxylation or calcination temperature, the carbonate phase in the solid sample was identified and the extent of carbon mineralization was determined. Detailed information on the estimation of the extent of carbonation can be found in the ESI.† During the TCA run, samples were placed in a ceramic boat and combusted in the presence of O_2 at temperatures as high as 1000 °C. The combustion process converts all carbon species – both inorganic and organic – into CO_2 and CO, and the total carbon is reported. In this study, both the TCA mode and TGA techniques were used to estimate the extents of carbon mineralization, and the results of both methods were compared to assess consistency. The crystalline phases present in the alkaline sorbents, catalysts and reaction products were detected using X-ray diffraction (XRD, Bruker D8 Advance ECO powder diffractometer, Bruker with Cu Kα radiation (40 kV, 25 mA)). The samples were scanned over the 2θ range from 20° to 80°. The FTIR spectra of powder and liquid samples were recorded with a FTIR spectrometer (ThermoFisher Scientific). Thirty-two scans were collected for each measurement in the spectral range of 4000–400 cm^{-1} with a resolution of 4 cm^{-1} and the average was taken as a representative measurement. Fig. S2a† presents the FTIR spectra corresponding to various oxygenates for a baseline comparison.

Determination of the morphological features of the solid samples. The particle size distributions of the materials were determined using a particle size analyzer (Anton Paar). Fig. S3(a)† presents the particle size distribution of ladle slag. The pore size distributions (PSDs), surface areas, and pore volumes of the starting materials and synthesized particles were determined from N_2 adsorption–desorption isotherms using the Brunauer–Emmett–Teller technique (BET) (Quantachrome Autosorb iQ Analyzer, Boynton Beach, FL). Before measuring the adsorption–desorption isotherms, the synthesized samples were outgassed at 120 °C for 24 h. The total pore volume, average pore diameters and pore size distributions were obtained from the N_2 adsorption branches of isotherms using the Barrett–Joyner–Halenda (BJH) method.

Determination of the chemical compositions of liquids using NMR spectroscopy. The compositions of the oxygenate molecules were determined using nuclear magnetic resonance (NMR). NMR data were acquired on a 500 MHz Bruker AVIII spectrometer equipped with a Prodigy BBO probehead. To calculate the mass composition, ^1D and ^1H spectra were acquired with 4 scans, 30 seconds relaxation delay, 10 kHz spectral width, and 3.3 s acquisition time. The spectra were processed in MNova (version 14.2.3, Mestrelab Research S.L.). The FIDs were zero filled to 128k points prior to Fourier transform. Automatic phase correction was applied followed by baseline correction with 5th-order Bernstein polynomials. Spectra were superimposed and frequency aligned using solute signals, and integrated using automatic linear correction for solute signals. Minor products were identified by suppressing the water signal using WET as implemented in TopSpin 3.6.4 (Bruker BioSpin). WET-1H spectra were acquired with 64 scans, 3 seconds relaxation delay, 8 kHz spectral width, and 2 s acquisition time. Fig. S2b† presents the NMR spectra corresponding to various oxygenates for a baseline comparison.

2.2 Experimental setup

The experiments to investigate enhanced H_2 recovery from aqueous biomass oxygenates were conducted in a stainless-steel stirred reactor (Micro Bench Top Reactor, Parr Instrument Company), maintained at a temperature of 240 °C (± 5 °C), 50 bar (±1 bar) N_2 pressure, and stirring rate of 10 rpm (±2 rpm). Fig. 2(A) shows a schematic representation of the reactor system. Aqueous biomass oxygenates with a composition of 3 wt% were prepared by mixing high purity oxygenates in an appropriate volume of distilled water, and 3 g (±0.05 g) of either the Ni or Pt on alumina catalyst was used in the experiments that required a catalyst. Experiments were also performed without a catalyst as the base case. Prior to the start of each experiment, the system was purged with N_2 for 3–5 min to remove any trapped gas impurities. The system was then heated, and the gas pressure was set to the desired value. The start of the reaction was marked by reaching the desired temperature setpoint of 240 °C (±5 °C). At the end of the reaction, the reactor was cooled back to room temperature, and the products were collected and analyzed.

The product gases were analyzed by connecting the reactor to a gas chromatograph (GC) equipped with four columns connected in series (MS and Poraplot Q) with thermal conductivity and flame ionization detectors (TCD-FIDs). H_2, O_2, N_2, CH_4 and CO were analyzed using channel A with a molecular sieve column and argon as the carrier gas; CO_2, C_2H_4, and C_2H_6 were analyzed using channel B with a molecular sieve column and helium as the carrier gas. The gas sample was injected after every experiment was completed. Since the concentration of inert gas, N_2, is already known at the start of the reaction, the concentrations of product gases were calculated based on the N_2 concentration in the gas samples. For each reaction condition, an error bar was generated by using 3–4 repeated experiments. The gas yields were obtained by GC analysis and their purities were calculated from the volume concentration ratio. Known concentrations of standard gases, *i.e.*, H_2, CO, CO_2, and hydrocarbon gases were used as calibration gases.

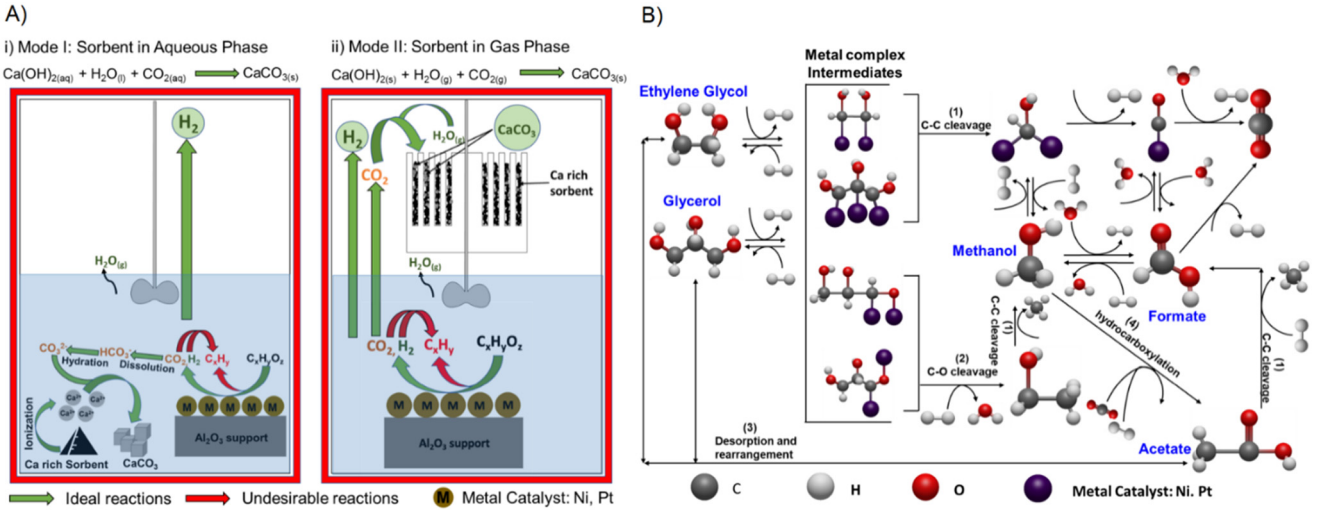

Fig. 2 (A) Reaction configurations for H_2 evolution with *in situ* CO_2 capture and mineralization. In mode I, the catalyst, alkaline sorbent, and oxygenate feedstock are mixed to form a slurry. In mode II, the alkaline sorbent is suspended in the gas phase, while the catalyst and feedstock are mixed in the liquid phase. (B) Reaction pathways associated with the deconstruction of oxygenates to produce H_2 from aqueous biomass oxygenates are shown.

H_2 evolution was also studied by exploring two distinct modes of operation. In mode I, the biomass oxygenates, alkaline sorbent (calcium hydroxide), and catalyst are co-present as a slurry. In mode II, a basket bearing the alkaline sorbent is in contact with the gas phase and the fluid phase (oxygenate–water mixture) remains in contact with the catalyst. Placing the catalyst in the aqueous phase and the alkaline sorbent in the gas phase enables ease of recovery and reuse of the catalyst. The hypothesis that reactivities will differ in modes I and II due to differences in mass transfer behavior was investigated. For example, in mode II, CO_2 exsolution into the gas phase is essential for *in situ* CO_2 capture unlike in mode I, where CO_2 in the aqueous phase can be directly captured to produce solid carbonates. In both modes, the solid products were recovered and separated from the liquid mixture using vacuum filtration and dried in a vacuum oven. The recovered solids were analyzed for carbonate content, and their structural and morphological features. The liquid products and catalysts before and after reactions were also characterized to determine changes in chemical composition.

2.3 Extent of carbon mineralization and product yield calculations

The extent of carbon mineralization is defined as the measured amount of CO_2 stored in the samples as solid carbonate relative to the theoretical maximum CO_2 storage capacity based on the stoichiometry of complete conversion and is expressed by eqn (1):

$$\text{Extent of carbon mineralization (\%)} = \frac{\text{measured amount of } CO_2 \text{ in the samples}}{\text{theoretical maximum } CO_2 \text{ storage capacity}} \times 100 \quad (1)$$

More information on the chemical phase determination and extent of carbon mineralization of heterogeneous slag samples can be found in the ESI.†

The conversion of biomass oxygenates and associated yields of products (*e.g.*, H_2, CO, CH_4, and CO_2) are determined using eqn (2)–(4) as shown below.

$$\text{\% Conversion of Biomass Oxygenates (BO)} = \frac{BO_{in} - BO_{out}}{BO_{in}} \times 100 \quad (2)$$

$$\text{\% } H_2 \text{ yield} = \frac{\text{Moles of } H_2 \text{ produced}}{\text{Moles of biomass oxygenate fed} \times \text{Stoichiometric Ratio(SR)}} \times 100 \quad (3)$$

$$\text{\% CO, } CO_2 \text{ and alkanes yield} = \frac{\text{Moles of C in compound produced}}{\text{Moles of C atoms in BO fed}} \times 100 \quad (4)$$

The stoichiometric ratio (SR) is a factor obtained from the stoichiometry for complete conversions of biomass oxygenates as shown in Table S1 in the ESI.†

3. Results and discussion

3.1 Pathways involved in enhanced H_2 recovery with inherent carbon removal from aqueous biomass oxygenates

The three key multiphase reactions involved in producing H_2 with *in situ* CO_2 capture from aqueous biomass oxygenates are: (i) the deconstruction of the oxygenates over a metal catalyst, (ii) the selective cleavage of C–C or C–O cleavage to produce $CO/H_2/CO_2$ and CH_4 over a metal catalyst, respectively, and (iii) the reactivity of CO_2 with Ca- or Mg-

oxides or hydroxides to produce Ca- or Mg-carbonates. Robust characterization of multiphase gas–liquid–solid chemical interactions is crucial for delineating which of these steps is rate-limiting.[28,49] In the first step, the oxygenates typically undergo reversible dehydrogenation over a metal catalyst to produce adsorbed intermediates, prior to cleavage of C–C and C–O bonds. The reaction pathways involved in the deconstruction of aqueous biomass oxygenates are shown in Fig. 2(b).

When considering the deconstruction mechanisms of glycerol and ethylene glycol, the first pathway usually involves the cleavage of the C–C bonds leading to the formation of CO and H_2. This pathway is ideal for producing adsorbed CO for water gas shift reactions in the subsequent step. However, when the starting feedstock is acetate, the cleavage of the C–C bond typically leads to the formation of CO, H_2 and CH_4. Another reaction pathway involves the cleavage of C–O bonds followed by hydrogenation with ethylene glycol and glycerol precursors to produce an alcohol. The alcohol can further react on the metal surface *via* adsorption, C–C bond cleavage or C–O bond cleavage which can lead to the formation of CH_4, CO_2, H_2 and H_2O. Another possible pathway involves the desorption of species from the metal surface followed by rearrangement (which may occur on the catalyst support and/or in the aqueous phase) to form an acid, which can then undergo surface reactions including adsorption, C–C bond cleavage, and C–O bond cleavage to form alkanes (*e.g.*, CH_4, C_2H_6), CO_2, H_2 and H_2O. These interactions highlight the selectivity challenges that exist in tuning multiphase chemical interactions for preferentially synthesizing CO, CO_2, and H_2 over alkanes or alcohols. It has been shown that slightly acidic solutions promote alkane formation due to acid-catalyzed dehydration reactions, followed by hydrogenation on the metal interface. In contrast, neutral and basic solutions yield high H_2 and low alkane selectivities[49] Therefore, the hypothesis, in which alkaline environments bearing calcium hydroxide or oxide aid in the selective deconstruction of biomass oxygenates to produce H_2, is investigated in this study.

The second potentially rate-limiting step involves the selectivity of gas phase chemical reactions to producing CO_2 and H_2 *via* the water gas shift reaction (see reaction (2)) as opposed to methanation reactions (see reactions (3) and (4)) which result in CH_4 evolution. Methanation reactions scavenge H_2 to produce CH_4, which is not desirable. Examples of other possible reactions that limit H_2 yields include alcohol dehydration, which produces large amounts of hydrocarbons, CO/CO_2 reduction and Boudouard reactions which lead to the formation solid carbon.[28] Acidic environments arising from the evolution of CO_2 and dissolution aid in methanation. However, the hypothesis that alkaline environments, such as those with the presence of $Ca(OH)_2$, aid in CO_2 removal and suppress methane evolution has not been extensively explored. Furthermore, according to the Le Chatelier principle,[50] the removal of CO_2 promotes an equilibrium shift in the WGS reaction (reaction (2)) to favor more rapid H_2 production and CO consumption which simultaneously impede the formation of methane (reactions (3) and (4)).

$$CO + H_2O \rightarrow H_2 + CO_2 \quad (R2)$$

$$CO + 3H_2 \rightarrow CH_4 + H_2O \quad (R3)$$

$$CO_2 + 4H_2 \rightarrow CH_4 + 2H_2O \quad (R4)$$

The third and final step is the removal of CO_2 from the gaseous phase *via* carbon mineralization using alkaline sorbents such as Ca- or Mg-hydroxides and alkaline industrial residues (*e.g.*, ladle slag generated during steel making) to produce stable solid carbonates with limited solubility in water. The dissolution of Ca- or Mg-hydroxides or oxides mobilizes Ca^{2+} or Mg^{2+} ions which can react with dissolved carbonates to produce solid Ca- or Mg-carbonates, as shown in reactions (5)–(9). The pH of our feedstock was found to increase from 4.88–7.67 to 12.25–12.29 post-addition of $Ca(OH)_2$ and 12.15–12.19 post-addition of the LD sorbent (see Table S4†). Carbonate (CO_3^{2-}) concentrations that are needed for carbon mineralization are favored over bicarbonate ions (HCO_3^-) with an increase in pH (see Fig. S4†), which favors the formation of solid carbonates as shown in reactions (8) and (9).

Dissolution of Species

$$Ca(OH)_2 \rightarrow Ca^{2+} + 2OH^- \quad (R5)$$

$$Mg(OH)_2 \rightarrow Mg^{2+} + 2OH^- \quad (R6)$$

$$H_2O + CO_2 \rightarrow CO_3^{2-} + 2H^+ \quad (R7)$$

Carbonate Formation

$$Mg^{2+} + CO_3^{2-} \rightarrow MgCO_{3(s)} \quad (R8)$$

$$Ca^{2+} + CO_3^{2-} \rightarrow CaCO_{3(s)} \quad (R9)$$

Despite the simplicity of the stoichiometric reactions describing the formation of Ca- or Mg-carbonates, complex chemo-morphological interactions result in non-monotonic kinetics of carbonate nucleation and growth. For example, the kinetics of carbon mineralization are strongly influenced by the pH and composition of the aqueous phase,[51] partial pressure of CO_2,[52] and temperature.[34] pH conditions greater than 8 favor (bi)carbonate formation which aid in solid carbonate formation while more acidic pH conditions favor the dissolution of Ca- or Mg-oxides and hydroxides. Higher CO_2 partial pressures coupled with alkaline aqueous environments favor CO_2 solvation and carbon mineralization.[36] Elevated temperatures favor the dissolution of Ca- or Mg-oxides and hydroxides and thermodynamically favor the precipitation of solid carbonates.[36] While the thermodynamic feasibility of realizing CO_2 removal *via*

carbon mineralization when coupled with the deconstruction of biomass oxygenates has been established,[28] the associated kinetics have not been discussed.

CO_2 removal *via* carbon mineralization can be integrated with the deconstruction of biomass oxygenates in two modes. In the first mode, the aqueous biomass oxygenates, catalyst, and alkaline sorbent are actively interacting in a slurry environment. In this mode, any evolved CO_2 can be rapidly mineralized to produce solid carbonates when excess alkalinity is present. This approach, if successful, can limit the exsolution of CO_2 into the gas phase. However, carbonate formation on the catalyst in the aqueous phase can lead to deactivation. Alternatively, another mode can be explored in which the alkaline sorbent can be placed in the gas phase. In this mode, the deconstruction of biomass oxygenates in the aqueous phase results in the exsolution of CO_2 into the gas phase followed by mineralization. The mass transfer of CO_2 from the aqueous phase to the gas phase, followed by the reaction of CO_2 with the alkaline sorbent suspended in the gas phase, introduces additional "resistances" to *in situ* CO_2 capture and removal. However, this mode has a significant advantage where catalysts are not deactivated by solid carbonate formation, and *in situ* separation of solid carbonate products from the deconstructed aqueous biomass oxygenate-bearing solutions and solid catalysts can be easily achieved. Thus, the experiments conducted in this study and discussed in the following sections are designed to examine the influence of these coupled multiphase chemical interactions on enhanced H_2 recovery with inherent carbon removal, with the intent to inform appropriate reaction modes for scalable deployment.

3.2 Carbon removal effect on H_2 evolution during the non-catalyzed hydrothermal treatment of oxygenates

Chemical reactions that proceed *via* cleavage of covalent bonds in organic compounds usually have high activation energies. Hence, these pathways typically require a catalyst to lower their activation energy for the reactions to occur fast enough over short time scales. In this study, a base case scenario involving the hydrothermal conversion of 3 wt% methanol was conducted to elucidate the effect of coupling mineralization reactions without a catalyst on the reforming process. In the absence of a catalyst and an alkaline sorbent for *in situ* CO_2 capture, H_2 yields obtained are less than 1% after a reaction time of 3 hours (Fig. 3). These low H_2 yields of $<1\%$ are consistent with the thermodynamic calculations reported in our prior studies.[28] However, unlike predictions from thermodynamic studies, hydrocarbons such as CH_4 are not detected in the gas product stream for all cases studied in the absence of a catalyst. The results from product liquid analyses using NMR in Fig. 3(B) show formate and acetate as the only intermediates formed when methanol is the oxygenate precursor. From this observation and the absence of hydrocarbons in the product gas stream, we infer that without a catalyst, H_2 production from methanol is likely to proceed solely *via* the formation of formate as shown in Fig. 2(B). In the formate pathway, methanol undergoes partial oxidation to produce formate, which further produces CO_2 and H_2 *via* dehydrogenation. Although no gaseous CO was observed in the product gas stream, we cannot completely rule out the possibility of the formation of CO intermediates *via* the CO pathway. In the future, *operando* measurements will be conducted to evaluate this hypothesis.

Over an extended reaction residence time, we observed an increase in the concentration of acetate in solution (Fig. 3(B)), which could be due to the recombination of CO_2, H_2 and methanol *via* hydrocarboxylation to produce acetate.[53] The preferential formation of acetate through hydrocarboxylation rather than methane formation *via* methanation is a very interesting observation, especially since H_2 and CO_2 have been extensively reported to be thermodynamically unstable compared to alkanes and water at low temperatures.[49] Overall, the kinetics of H_2 evolution without a catalyst was observed to be greatly limited by biomass deconstruction to produce H_2 as opposed to the formation of undesired products such as methane formation.

Further, we observed that the H_2 and CO_2 yields increase, although very slowly with time (Fig. 3(A), (C) and (D)). In the presence of $Ca(OH)_2$ for CO_2 capture, a slight relative increase in H_2 yields in the range of 0.1–4.8% were achieved under similar conditions. While these results show the importance of an alkaline environment in enhancing these reactions, it is also evident that without a catalyst, these systems are severely limited by biomass deconstruction with or without an alkaline sorbent. These results clearly demonstrate that catalysts are essential for biomass oxygenate deconstruction, and their absence can severely limit H_2 evolution even when coupled with exothermic carbon mineralization reactions.

3.3 Effect of catalysts on enhanced H_2 yield without *in situ* CO_2 removal

High yield and selectivity for H_2 production from aqueous oxygenates are challenging to achieve without an appropriate catalyst. To address this challenge, both Pt/Al_2O_3 and Ni/Al_2O_3 are selected for this study, given their effectiveness in the reforming of heavy oxygenated hydrocarbons due to their high activity for C–C cleavage.[49] The Ni/Al_2O_3 catalyst shows better activity for both C–C breakage and water gas shift reaction compared to the Pt/Al_2O_3 catalyst,[8,49,54] However, a better catalyst performance implies that the catalyst must also not facilitate undesired side reactions such as methanation. Fig. 3(C) and (D) show that H_2 yields of 20% are achieved in the presence of Ni/Al_2O_3 catalysts with 3 wt% methanol after 1 hour of reaction time and at 240 °C. Under similar conditions, about a 60% H_2 yield was obtained using Pt/Al_2O_3. The lower H_2 yield obtained with Ni/Al_2O_3 corresponds to the higher relative amount of methane

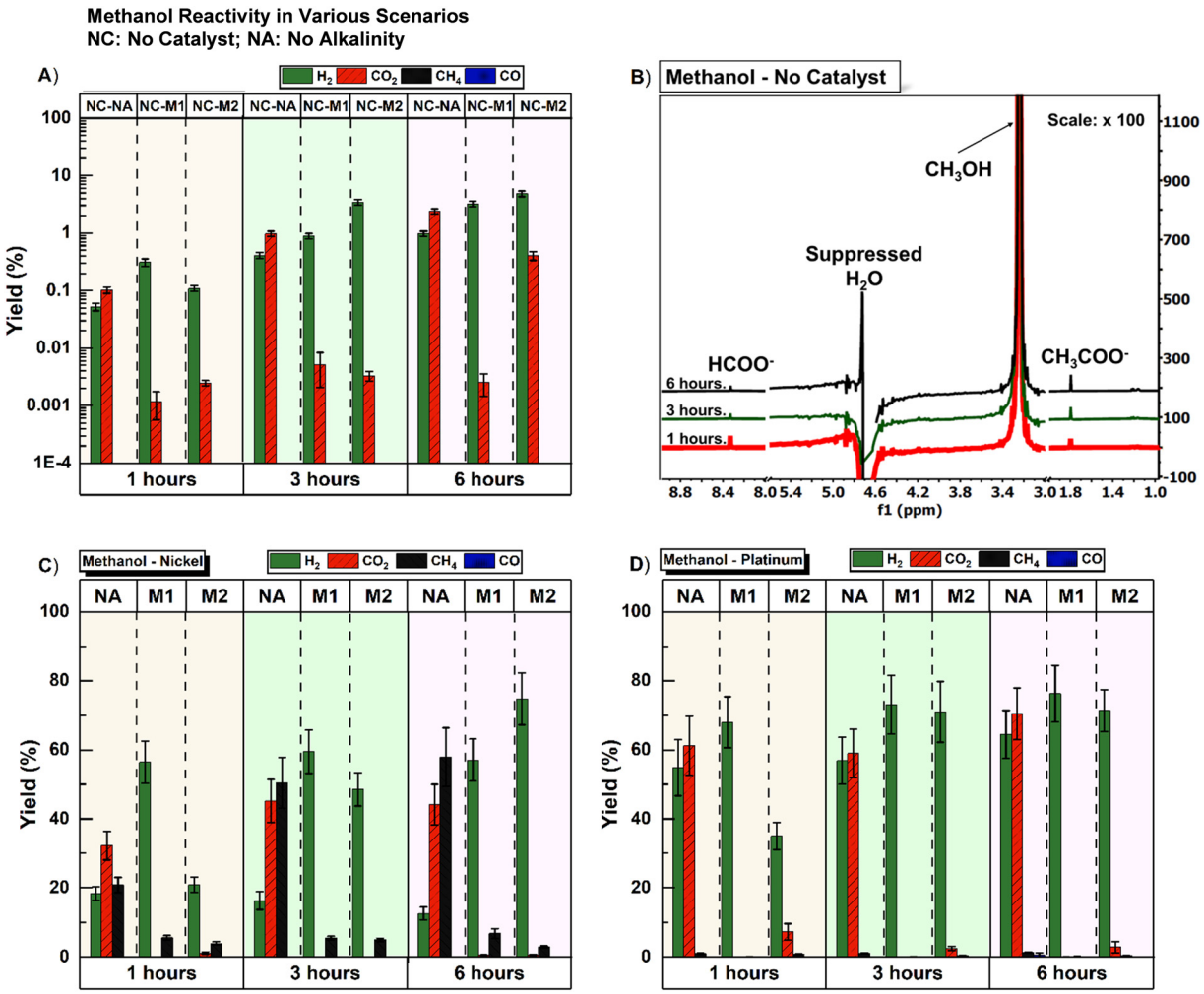

Fig. 3 (A) Gas product yield for base case (without a catalyst) H_2 production from the hydrothermal treatment of 3 wt% methanol with and without an alkaline sorbent ($Ca(OH)_2$). (B) H_2O suppressed NMR spectra of liquid products from temporal evolution resulting from the deconstruction of oxygenates in the presence of alkaline sorbents in contact with the fluid phase (mode I). Only the dominant vibrations are labeled, and the spectra are offset for clarity. (C) Product yields in the gas phase when the Ni/Al_2O_3 catalyst is used during the hydrothermal treatment of 3 wt% methanol with and without an alkaline sorbent ($Ca(OH)_2$). (D) Product yields in the gas phase when the Pt/Al_2O_3 catalyst is used during the hydrothermal treatment of 3 wt% methanol with and without an alkaline sorbent ($Ca(OH)_2$). Alkaline sorbent reactions are carried out in mode I (catalyst, sorbent and feedstock are mixed to form a slurry) and mode II (sorbent is suspended in the gas phase, while the catalyst and feedstock are mixed in the liquid phase), at temperatures of 240 °C and pressures of 50 bar N_2. NA: no alkalinity, NC: no catalyst, M1: mode I, and M2: mode II.

produced. We observed that a 25% yield of methane was produced with Ni/Al_2O_3, whereas methane yields of <1% were realized with Pt/Al_2O_3 (Fig. 3(C) and (D)). These observations of high H_2 selectivity with Pt/Al_2O_3 are consistent with other studies reported in the literature.[55] On this basis, Pt-based catalysts have been consistently identified as a better catalyst for H_2 production. Regardless, the earth abundance, low cost, and high biomass deconstruction activity provided by Ni-based catalysts are desirable for the deconstruction of aqueous biomass oxygenates.

Longer reaction times of 6 hours increased the CH_4 yield from methanol as the precursor as shown in Fig. 3(C) and (D). An increase in CH_4 yield from 0.99% to 1.4% is observed when the reaction time was increased from 1 hour to 6 hours in the presence of the Pt/Al_2O_3 catalyst. The corresponding increase in CH_4 yield in the presence of the Ni/Al_2O_3 catalyst from 20.7% to 58% is more prominent. A simultaneous decrease in H_2 yield observed in Fig. 3(C) and (D) confirms that methane formation occurs primarily due to gas phase selective reactions of CO/CO_2 favorable under these conditions. Longer residence times imply more time for methane formation due to the increase in CO_2 concentration. NMR analyses of the liquid products shown in Fig. S5–S7 in the ESI† confirm the presence of very low quantities of formate and acetate using either the Pt or Ni catalyst, thus supporting our earlier hypothesis that these reactions also proceed *via* the formate formation route in Fig. 2(B). These results also show that H_2 and CO_2 do recombine with methanol *via* hydrocarboxylation to produce acetate.

However, in the presence of a catalyst, H_2 and CO_2 recombine more selectively to produce methane as shown in reaction (4). Faster methanation on the Ni catalyst relative to that on Pt is consistent with the lower activity of the Pt catalyst for methanation reactions.

To obtain additional insights into the influence of catalyst morphology on reactivity, the pore sizes and morphologies are determined using BET analyses. The specific surface area (SSA), pore volume, and average pore diameter of the raw and spent Ni/Al_2O_3 and Pt/Al_2O_3 catalysts are reported in Table 2. The BET surface area of raw Ni/Al_2O_3 catalyst (259.080 ± 2.2% m^2 g^{-1}) synthesized in the lab was found to be higher than that of raw Pt/Al_2O_3 (174.375 ± 2.2% m^2 g^{-1}). This observation is attributed to the relatively smaller sizes of Al_2O_3 particles in the Ni/Al_2O_3 catalysts synthesized in the lab. The number weighted average particle size of the Ni/Al_2O_3 catalyst is 40 nm, which is considerably lower than that of Pt/Al_2O_3 which is 200 nm as shown in Fig. S8a in the ESI.† Post-reaction, we observed a significant decrease in the surface area of the Ni/Al_2O_3 and Pt/Al_2O_3 catalysts. This is likely due to transformation of the catalyst and catalyst support; in particular, the hydration of Al_2O_3 to form boehmite was evident as shown in Fig. S9 and S10 in the ESI.† While the loading of Pt and Ni on the Al_2O_3 support is the same at 5 wt%, we do not eliminate the possibility that morphological features such as the particle size, pore size and surface area of a catalyst could potentially impact methane selectivity. Formation of methane from aqueous phase reforming of butanol over Rh/ZrO_2 was recently found to decrease from 0.25 mol CH_4 per mol feedstock to 0.01 mol CH_4 per mol feedstock as the catalyst particle size increased from 40–60 μm to 250–420 μm, after 2 hours of reaction.[25] Lower conversions of feedstocks were observed due to these morphological changes in the catalyst particles. In contrast, an ideal scenario would be one where lower methane yields can be achieved while maintaining high conversions of biomass oxygenates to desired gaseous products such as H_2.

3.4 Enhanced catalytically aided H_2 evolution with *in situ* carbon removal

While our work reported in the previous section, supported by extensive prior research,[17,18,28,42,56] has shown that catalysts are essential for deconstructing biomass oxygenates to produce CO_2 and H_2, the hypothesis that *in situ* CO_2 capture and removal will enhance H_2 yield (as shown in reaction (1)) remains unexplored. To investigate the influence of alkaline sorbents, which is calcium hydroxide ($Ca(OH)_2$) in this case, experiments were performed at temperatures of 240 °C and pressures of 50 bar N_2 using 3 wt% methanol solution. The results are summarized in Table S2† and Fig. 3.

Fig. 3 shows that in the presence of $Ca(OH)_2$, the methane yields are suppressed with either the Ni/Al_2O_3 or Pt/Al_2O_3 catalyst. CH_4 yields of about 6% were obtained with Ni/Al_2O_3, when $Ca(OH)_2$ was used for *in situ* CO_2 capture, which showed a significant decrease from ~58% obtained without *in situ* CO_2 capture after 6 hours of reaction. In contrast, the CH_4 yield decreased from ~1.3% to ~0.4% using Pt/Al_2O_3, with and without *in situ* CO_2 capture. CO_2 removal *via* solid carbonate formation leads to the depletion of CO_2 in the product stream and favors CO consumption as a reactant which limits methane formation. The results showing CH_4 suppression using Pt/Al_2O_3 are not as significant as the results obtained with Ni/Al_2O_3 due to the relatively lower activity of Pt/Al_2O_3 for methanation reactions as shown in reactions (3) and (4). Higher selectivity for H_2 with Pt/Al_2O_3 catalysts is consistent with prior studies on biomass oxygenate deconstruction to produce H_2.[49] Interestingly, H_2 yields as high as 74% are achieved in mode II configuration in which $Ca(OH)_2$ is placed in the gas phase, as opposed to 57% in mode I configuration in which $Ca(OH)_2$ is in the aqueous phase, for a reaction time of 6 hours using the Ni/Al_2O_3 catalyst. Similarly, in the presence of the Pt/Al_2O_3 catalyst, H_2 yields as high as 71% are achieved in mode II configuration when $Ca(OH)_2$ is placed in the gas phase, as opposed to 76% in mode I configuration in which $Ca(OH)_2$ is

Table 2 Surface area, pore size volume, and average pore diameter of the materials in this study

Samples	Surface area[a] (m^2 g^{-1})	Pore size volume[b] (cc g^{-1})	Average pore diameter[c] (nm)
Alkaline feedstock ($Ca(OH)_2$)	31.35	0.13	3.85
Raw catalyst (Ni)	259.08	0.42	6.30
Raw catalyst (Pt)	174.37	0.28	5.83
Catalyst (Ni) + $Ca(OH)_2$	174.18	0.30	6.29
Catalyst (Pt) + $Ca(OH)_2$	112.94	0.20	5.83
Product ($CaCO_3$)	8.38	0.02	2.75
Used catalyst (Ni)	30.53	0.10	3.92
Used catalyst (Pt)	15.69	0.10	3.07
Used catalyst (Ni) + product ($CaCO_3$)	10.83	0.07	4.00
Used catalyst (Pt) + product ($CaCO_3$)	9.18	0.04	2.99
Ladle slag	9.18	0.03	3.84
Ladle slag after reaction	38.41	0.08	3.85

[a] Calculated using the BET equation. [b] BJH pore desorption volume. [c] Desorption average pore diameter. Measurements are reported within a BET error range of ±2.2%.

in the aqueous phase. Furthermore, longer reaction times of up to 6 hours enhance H_2 yields in the presence of the Ni/Al_2O_3 catalyst and in modes I and II. In contrast, increasing the reaction time from 3 to 6 hours does not result in a significant enhancement in H_2 yield in modes I and II in the presence of the Pt/Al_2O_3 catalyst. CO_2 concentrations in the product stream are negligible after reaction times of 3 hours and 6 hours when the Ni/Al_2O_3 catalyst is used, and below 2% in the presence of the Pt/Al_2O_3 catalyst.

These results are significant for several reasons. First, the effectiveness of mode II in enhancing H_2 yields with significant suppression of CO_2 yields is unexpected. It was hypothesized that the direct contact of the aqueous phase with $Ca(OH)_2$ promotes the dissolution and rapid uptake of any carbonate-bearing species without releasing CO_2 into the gas phase. In contrast, our results show that the gas–solid contact of $Ca(OH)_2$ and CO_2 evolved during biomass oxygenate deconstruction is also effective in enhancing H_2 yields with *in situ* CO_2 capture. The low pH of the solution due to the absence of an alkaline sorbent in the aqueous phase could be responsible for facilitating CO_2 exsolution. Fig. S4† shows that the formation of H_2CO_3 (a precursor for CO_2 exsolution) is more prominent at low pH. These results demonstrate that *in situ* separation of carbonate-bearing products can be realized concurrently with enhanced H_2 yields. Interestingly, H_2 evolution increases monotonically with time in mode II unlike in mode I, in which higher reactivities are achieved immediately due to the rapid uptake of CO_2 by calcium hydroxide in the aqueous phase. In mode II, *in situ* CO_2 capture is the rate limiting step with longer reaction times contributing to higher yields.

Further, H_2 evolution is observed to increase monotonically with time in mode II. This result also makes sense as we had already established that the kinetics of biomass deconstruction reaction proceeds at this time in cases without an alkaline sorbent. Also, if the reaction proceeds *via* the CO pathway as shown in Fig. 2(b), the rapid increases of H_2 and CO_2 partial pressures coupled with the relatively lower void volume in mode II may also drive the reaction in the reverse direction at its early stages to increase the CO concentration in the reactor, hence leading to lower rates due to higher coverage of CO on the metal surface. Similar effects of CO on metal surfaces have been reported.[57] Faster CO_2 capture rates are obtained with mode I as shown in Fig. 4(B) and (D) which appears to be consistent with the faster kinetics observed with respect to the H_2 yield in Fig. 3. This fast kinetics in mode I appeared to slow down significantly after 60 minutes of reaction, which suggests that we could be experiencing mass transfer limitations likely due to the formation of insoluble carbonates on active catalyst sites, preventing further H_2 production.

Progressive increases in calcium carbonate content observed in modes I and II over the Ni and Pt catalysts shown in Fig. 4(B) and (d) are consistent with the observed calcium carbonate phases in X-ray diffraction patterns in Fig. 4(E). Stable calcite phases are formed as opposed to metastable aragonite or vaterite phases, which is consistent with higher temperatures aiding in the formation of stable solid carbonate phases. The stability of the catalyst support is another consideration during oxygenate reforming. From the XRD plots in Fig. 4(E) and S10(b),† we observed the conversion of the alumina (Al_2O_3) support to a less active crystalline boehmite (AlOOH) phase. The presence of acetate has been reported to be responsible for the deactivation of Pt and Ni on alumina catalysts by hydroxylation of the Al_2O_3 surface, which forms crystalline boehmite (AlOOH) and leads to catalyst deactivation.[20,58] The observations from XRD analyses are supported by the appearance of Al–O–H vibrations observed post reaction from the FTIR spectra in Fig. 4(F) and S10(a).† *In situ* separation of the spent catalyst and solid carbonate product with mode II can also be confirmed by the absence of Al–O–H vibrations and the strong presence of, C–O and C═O vibrations in the carbonate product obtained post reaction as shown in Fig. 4(F). Further evidence of the conversion of calcium hydroxide to calcium carbonate and the absence of the boehmite (AlOOH) phase in mode II unlike those in mode I is confirmed from thermogravimetric analysis (TGA) as shown in Fig. 4(A) and (C). In mode I with either the Ni/Al_2O_3 or Pt/Al_2O_3 catalyst and calcium hydroxide in the aqueous phase, three distinct weight loss regimes are noted in the ranges of 360–430 °C, 440–540 °C, and 550–800 °C, which correspond to the dehydration of $Ca(OH)_2$, the dehydration of AlOOH, and the dissociation of $CaCO_3$, respectively. In contrast, the dehydration of $Ca(OH)_2$ and the dissociation of $CaCO_3$ are noted in mode II. Further, the DSC curves confirm an endothermic profile associated with the weight losses observed in DTG curves.

3.5 Enhanced H_2 production with *in situ* carbon removal using heavier aqueous oxygenates

Feedstock variability and the associated uncertainty in mechanisms and kinetics have been challenges in adapting innovative routes for producing H_2 from biomass feedstocks with inherent carbon removal.[59] To address this challenge, we investigate the influence of heavier C_1–C_3 oxygenated hydrocarbons such as glycerol, ethylene glycol, acetate, and formate on enhancing H_2 yields with and without inherent carbon removal. These oxygenates were chosen because they can be readily obtained in large quantities from low value biomass feedstocks such as food or municipal waste generated in urban or rural environments, algal sources, and industrial wastewater polluted streams.[28] Experiments were conducted over the Pt/Al_2O_3 and Ni/Al_2O_3 catalysts at 240 °C and 50 bar N_2 pressure. Experiments were performed in mode II since it has been shown that high H_2 yields and selectivity are achieved with *in situ* separation of CO_2 as a solid carbonate and ease of catalyst recovery. Varying the feedstock has been shown to have a strong influence on H_2 selectivity due to differing deconstruction mechanisms. It has been reported that within the family of polyols, the hydrogen selectivity of aqueous phase reforming decreases

with increasing carbon number of the feed.[49] Therefore, the influence of these differing deconstruction mechanisms on H_2 yields with and without CO_2 removal from aqueous biomass oxygenates is investigated. The yields of H_2, CO_2, CH_4, CO, and $CaCO_3$ are shown in Fig. 5 and summarized in Table S2.†

In the absence of *in situ* CO_2 removal, H_2 yields of ~15%, 19%, 2%, and 45% are achieved in the presence of the Ni/

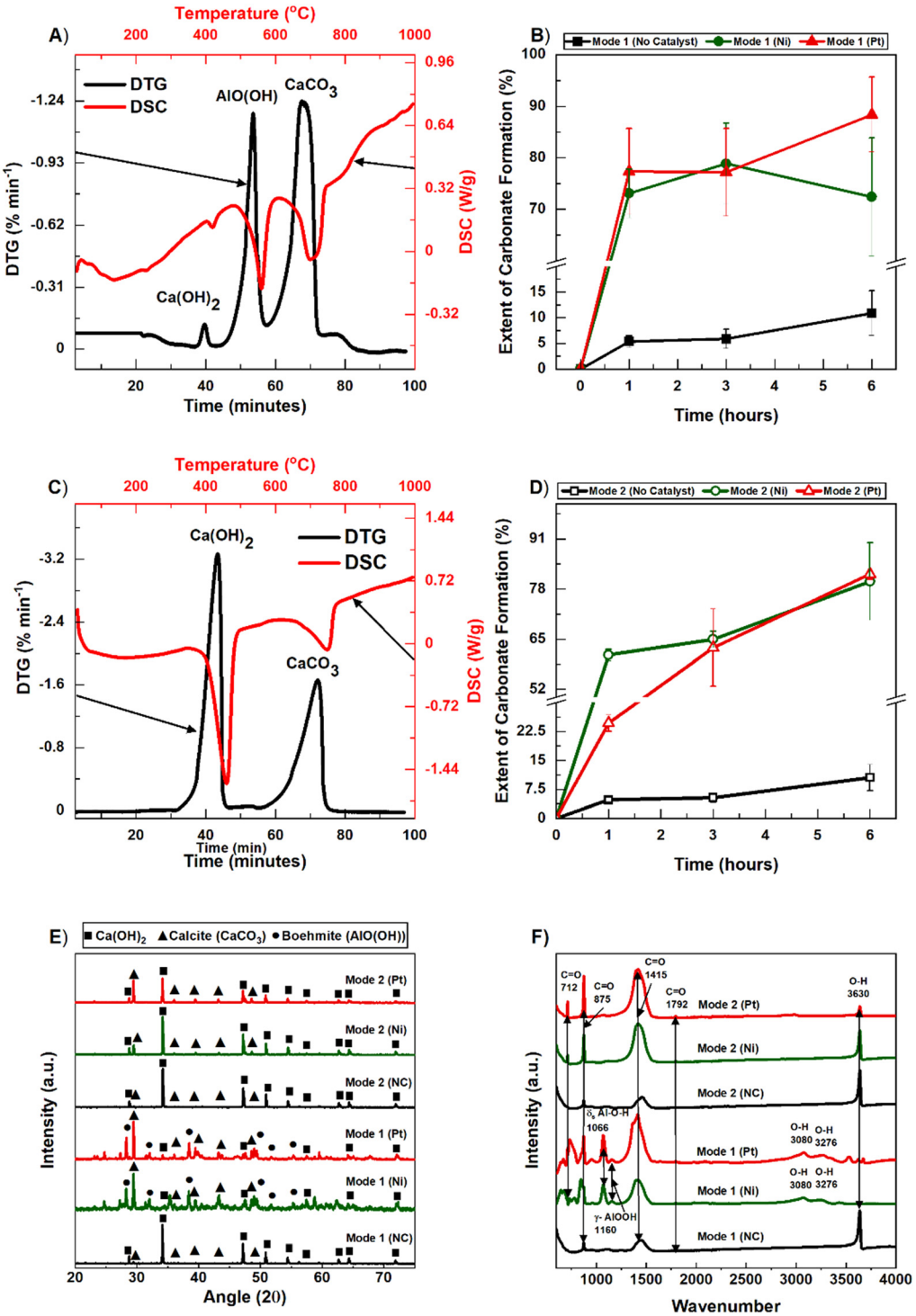

Fig. 4 Evidence of calcium carbonate formation in the solid product obtained from H_2 production *via* hydrothermal treatment of 3 wt % methanol based on: (A) thermogravimetric analysis of solid calcium carbonate product from mode I, (B) calculated extent of calcium carbonate formation in solid product obtained from mode I, (C) thermogravimetric analysis of solid product from mode II, (D) calculated extent of calcium carbonate formation in solid product obtained from mode I, (E) XRD analyses showing calcium carbonate phases formed post-reaction, and (F) FTIR analyses of solid calcium carbonate products obtained post-reaction.

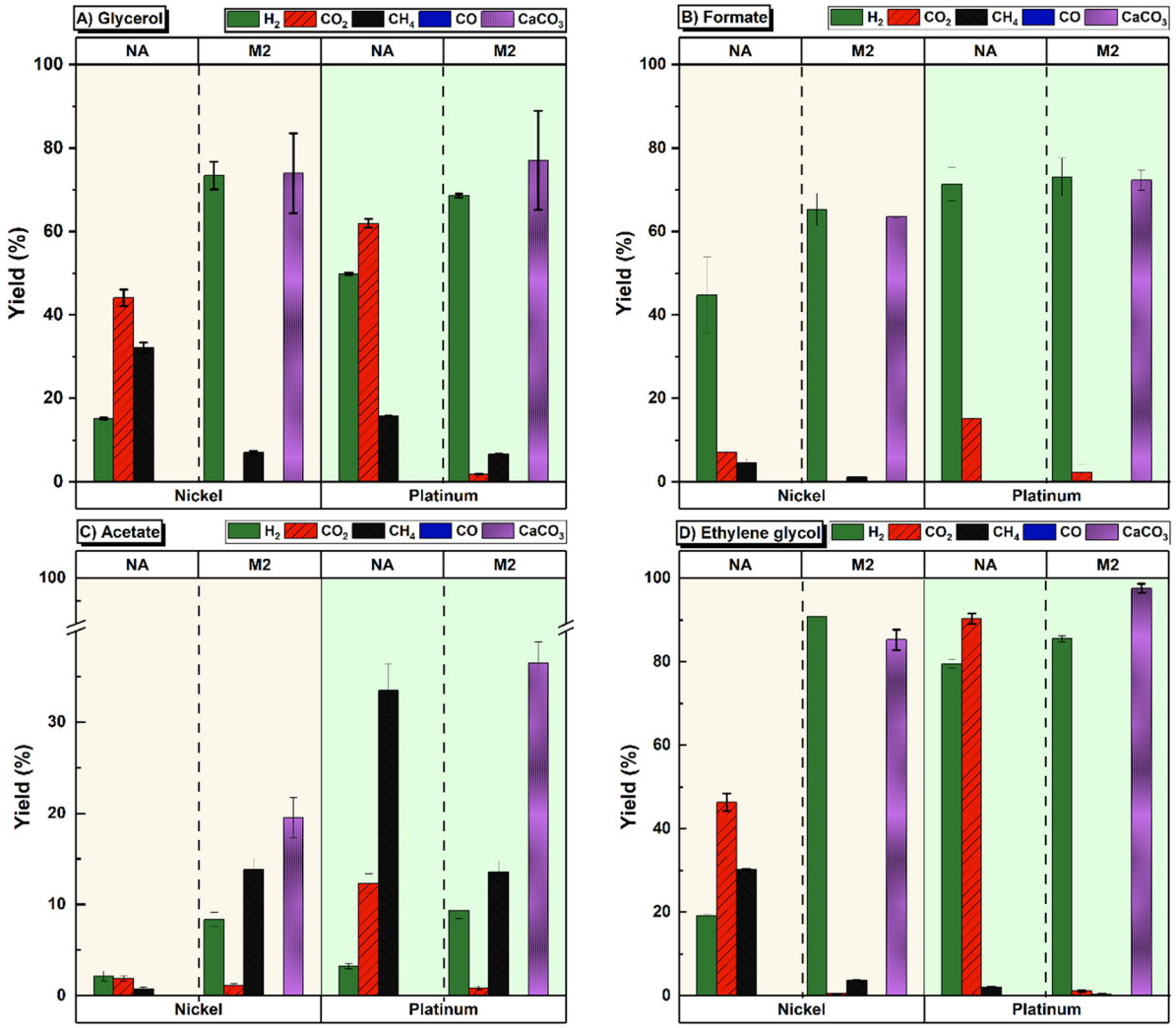

Fig. 5 Yields of H_2, CO_2, CH_4, CO, and $CaCO_3$ resulting from the hydrothermal conversion of 3 wt.% biomass oxygenates to H_2 with inherent carbon removal using the $Ca(OH)_2$ sorbent where (A), (B), (C), and (D) represent glycerol, formate, acetate, and ethylene glycol, respectively. NA represents the scenario when there is no alkalinity in the system. M2 represents mode II in which the alkaline sorbent is suspended in the gas phase, the catalyst and feedstock are mixed in the liquid phase, and the reaction temperature and N_2 pressure are 240 °C and 50 bar, respectively.

Al_2O_3 catalyst and ~49%, 79%, 3%, and 71% in the presence of the Pt/Al_2O_3 catalyst for glycerol, ethylene glycol, acetate, and formate, respectively. In contrast, the H_2 yields when coupled to *in situ* CO_2 removal are ~73%, 90%, 8%, and 65% in the presence of the Ni/Al_2O_3 catalyst and ~69%, 85%, 9%, and 73% in the presence of the Pt/Al_2O_3 catalyst for glycerol, ethylene glycol, acetate, and formate, respectively. Without *in situ* CO_2 capture, higher H_2 yields are consistently achieved with formate using either the Ni/Al_2O_3 or Pt/Al_2O_3 catalyst since H_2 production proceeds directly through the formate dehydrogenation pathway to produce H_2 and CO_2 as shown in Fig. 2(B). High H_2 yields are also accompanied by relatively lower methane yields of ~0.2% and 4.5% with Ni/Al_2O_3 and Pt/Al_2O_3, respectively, using formate as the starting feedstock. This is likely due to the elimination of possible methane formation *via* CO methanation as shown in reaction (3). Further, the formation of water-soluble sodium bicarbonate species from the interaction of bicarbonate and sodium ions in solution as shown in Table S1† prevents CO_2 production, and subsequently CO_2 methanation, which results in low yields of CO_2 and CH_4 (Fig. 5(B)). It is also interesting to note that formate is observed to be an intermediate liquid precursor using all oxygenates studied as starting feedstock. This was confirmed by NMR analyses on liquid products obtained post-reaction as shown in Fig. S7.†

In contrast, the lowest H_2 yields are achieved with acetate as the starting feedstock for several reasons. First, we can observe that either C–C or C–O bond cleavage of acetate results in the preferential formation of CH_4 prior to CO or CO_2 formation, which limits H_2 production (Fig. 2(B)). Second, the possibility of regenerating acetate *via* hydrocarboxylation also exists, which further leads to H_2 consumption.[53] Acetate has also been reported to be responsible for the deactivation of Pt–Ni catalysts by hydroxylation of the Al_2O_3 surface.[60] Subsequent re-deposition of the dissolved alumina on the catalyst causes

blocking of active catalytic Ni/Pt sites which leads to catalyst deactivation and hence limits feedstock conversion.[9] These results show that either biomass deconstruction or acetate regeneration could be limiting H_2 evolution and represents an interesting selectivity challenge that requires further investigation in our future work. H_2 yields of 20–80% are also noted with ethylene glycol and glycerol without *in situ* CO_2 capture, although higher methane formation was observed with glycerol. This is most likely due to the higher possibility of methane formation *via* C–O cleavage with glycerol relative to ethylene glycol, due to the presence of more O–H bonding sites for C–O cleavage in glycerol. Just as in the case of methanol, Fig. 5 also shows considerable methane suppression with *in situ* CO_2 removal with all biomass oxygenates except for acetate. Unsurprisingly, lower H_2 yields with acetate were observed even after coupling mineralization reactions in the presence of platinum and nickel catalysts. From the results shown in Fig. 5, we can infer that the selectivity for H_2 production improves in the order: acetate < glycerol < ethylene glycol ~ methanol < formate without *in*

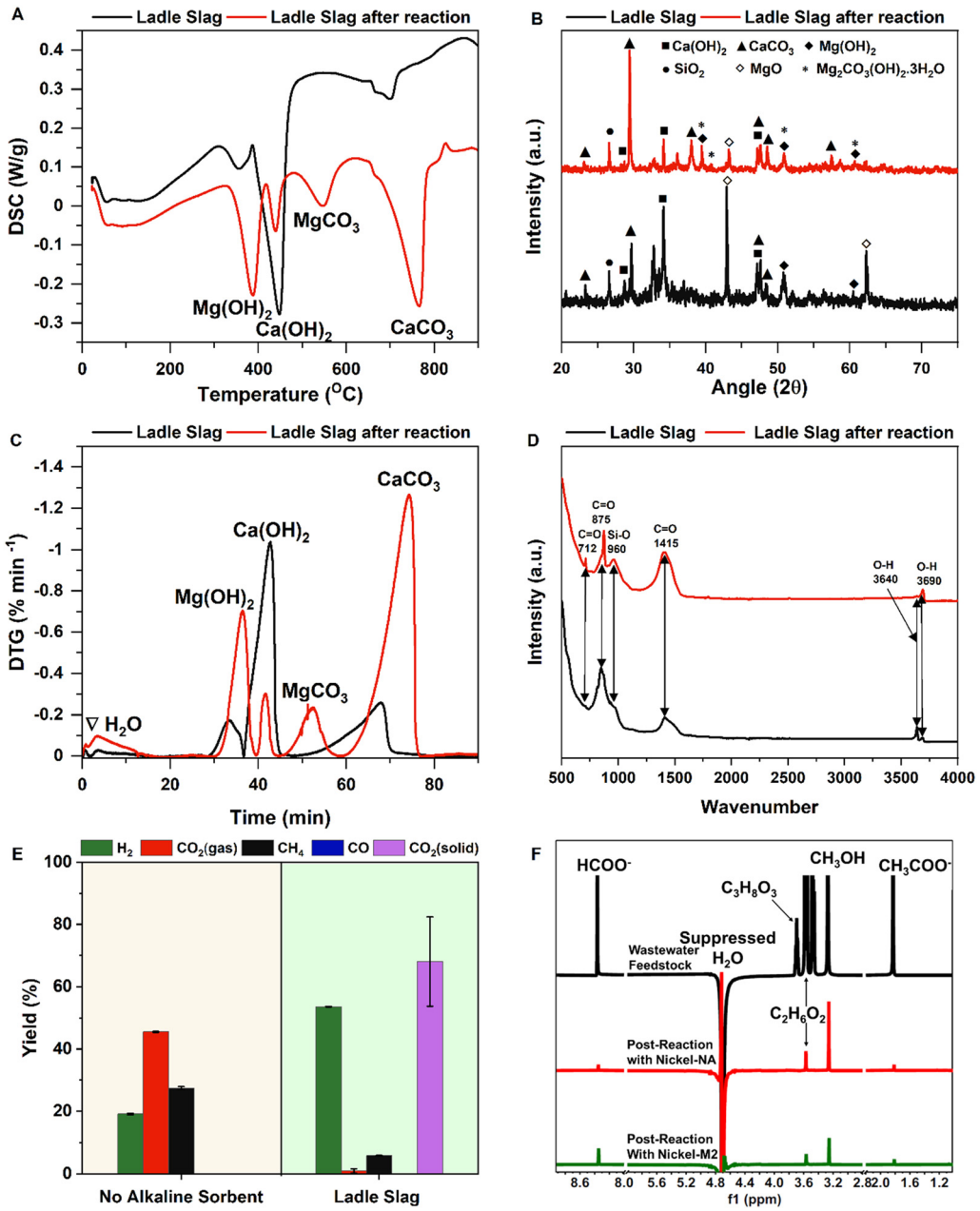

Fig. 6 Contrasting unreacted and reacted ladle slag obtained after H_2 conversion from model wastewater and CO_2 removal from ladle slag with *in situ* CO_2 capture using (A) DSC measurements, (B) XRD analyses, (C) DTG curves, (D) FTIR analyses, (E) product yields on using the Ni/Al_2O_3 catalyst, and (F) H_2O suppressed NMR spectra of liquid products. Only the dominant vibrations are labeled, and the spectra are offset for clarity in (F). Reactions are carried out in mode II where the sorbent is suspended in the gas phase, while the Ni/Al_2O_3 catalyst and mixture of biomass oxygenates are mixed in the liquid phase, at temperatures of 240 °C and N_2 pressure of 50 bar.

situ CO_2 capture and acetate < glycerol < methanol < formate < ethylene glycol with *in situ* CO_2 capture using the Ni and Pt on alumina catalysts. This trend was similar with the experimental results obtained *via* aqueous phase reforming by Davda and co-workers,[49] who reported that the order of biomass oxygenate reactivity is as follows: glucose < sorbitol < glycerol < ethylene glycol < methanol.

3.6 Model waste stream upcycling with carbon mineralization using alkali rich industrial residues

To probe the enhancement in hydrogen production from oxygenates using alkaline industrial residues, ladle slag was used as an alkaline sorbent in the presence of the Ni/Al_2O_3 catalyst. Model wastewater was also prepared in the lab using 3 wt% of a mixture of formate, acetate, glycerol, ethylene glycol and methanol to show the applicability of this process with heterogeneous streams. H_2 yields of 58% and 19% are observed with and without ladle slag, respectively. Further, methane suppression is also noted as the methane yields are reduced from 29% and 6% in the presence of ladle slag as an alkaline sorbent. We also detected an increase in the solid Ca- and Mg-carbonate content resulting from the capture and conversion of 70% of CO_2 released from the deconstruction of biomass oxygenates.

The solid product collected post-reaction is characterized by X-ray diffraction (XRD), as shown in Fig. 6(B). The main crystalline phases of fresh ladle slag are $Ca(OH)_2$ (portlandite), SiO_2 (silica), $Mg(OH)_2$ (brucite), and MgO (magnesia). Post reaction, a significant increase of peak intensities for $CaCO_3$ (calcite), and the appearance of phases such as $Mg_2CO_3(OH)_2{\cdot}3H_2O$ (artinite) are observed. Meanwhile, the peak intensities corresponding to both $Ca(OH)_2$ and MgO are significantly reduced. These results agree with the FTIR spectra analyses. Doublet O–H peaks at 3580–3650 and 3650–3720 cm^{-1} are observed in the FTIR spectrum of freshly milled ladle slag as shown in Fig. 6(D), which correspond to the vibrations from $Ca(OH)_2$, and $Mg(OH)_2$, respectively, and Si–O vibrations are also observed at 900–1000 cm^{-1}. The asymmetric stretching vibration band of C–O at 1420–1480 cm^{-1} and the bending vibration peaks of CO_3^{2-} at 873 and 712 cm^{-1} are prominent in the carbonate product. Post reaction, we observe a decrease in the intensity of $Ca(OH)_2$ and an increase in the intensity of $Mg(OH)_2$. This increase in O–H intensity associated with $Mg(OH)_2$ is due to both the synthesis of $Mg(OH)_2$ *via* the reaction of MgO with water, and the simultaneous formation of $Mg_2CO_3(OH)_2{\cdot}3H_2O$ *via* carbon mineralization of $Mg(OH)_2$. Further evidence of carbon mineralization is observed from the TGA plots in Fig. 6(A) and (C), which show four distinct weight losses corresponding to $Mg(OH)_2$, $Ca(OH)_2$, $MgCO_3$, and $CaCO_3$ respectively. These results conclusively demonstrate that the Ca- and Mg-bearing phases in ladle slag are the main reacting components with CO_2 to form the carbonate minerals, as shown by reactions (8) and (9).

4. Conclusion

This study has shown that high purity H_2 can be produced with inherent CO_2 removal from various biomass oxygenate sources including methanol, glycerol, ethylene glycol, acetate, and formate using alkaline industrial residues (ladle slag) as Ca- & Mg-bearing sources. As opposed to conventional high temperature reforming processes (>500 °C) at atmospheric pressure, we investigated the effect of maintaining fluids in the aqueous phase under a N_2 pressure of 50 bar and at a significantly lower temperature of 240 °C. Coupling aqueous phase biomass oxygenate reforming with thermodynamically downhill carbon mineralization reactions for *in situ* CO_2 capture successfully enhanced H_2 production. For example, ~90% *vs.* ~19% H_2 yield was obtained with and without *in situ* CO_2 capture respectively using ethylene glycol as starting feedstock, over a Ni/Al_2O_3 catalyst. Further, methane formation has been a long-standing challenge with Ni based catalysts. Our study also showed suppressed methanation rates (~4% *vs.* 30% CH_4 yield) with and without *in situ* CO_2 capture respectively using ethylene glycol as starting feedstock, over a Ni/Al_2O_3 catalyst. H_2 evolution is also studied using two modes of operations. While mode I, which favors the formation of carbonate species in solution, showed faster kinetics, *in situ* product separation is also shown to be achievable *via* mode II in which mineralization proceeds after CO_2 exsolution. H_2 yields as high as 79% and 74% are achieved using ethylene glycol and methanol in the presence of the Ni or Pt/Al_2O_3 catalyst and $Ca(OH)_2$ as an alkaline sorbent. Approximately 53% H_2 yield was obtained from a model C_1–C_3 carbon bearing wastewater stream using ladle slag as the alkaline sorbent, with over 70% of CO_2 released from the deconstruction of biomass oxygenates captured and converted as solid Ca- or Mg-carbonates. This study provides a novel pathway in which large amounts of low value residues such as Ca-rich alkaline residues and wastewater streams bearing biomass oxygenates can be successfully upcycled to produce high value H_2 with inherent CO_2 removal.

Author contributions

Conceptualization. G. G. and P. O.; data curation: G. G. and P. O.; formal analysis: G. G., P. O., S. M., A. M., and C. N.; funding acquisition: G. G. and P. O.; methodology: G. G. and P. O.; project administration: G. G.; resources: G. G. and P. O.; supervision: G. G.; visualization: G. G., P. O., S. M., A. M., and C. N.; writing – original draft: G. G. and P. O.; writing – review & editing: G. G., P. O., S. M., A. M., and C. N. All authors contributed to the discussion and provided feedback on the manuscript.

Conflicts of interest

There are no conflicts to declare.

Acknowledgements

The authors also acknowledge the use of the shared facilities at the Cornell Center for Materials Research (CCMR) which are supported through the National Science Foundation Materials Research Science and Engineering Centers (NSF MRSEC) program (DMR-1719875). G. G.'s contributions are supported by the DOE CAREER Award through the Office of Science DE-658308. P. O.'s efforts are supported by the Cornell Atkinson Small Grant Program through the Reducing Climate Risk initiative funded by the Cornell Atkinson Center for Sustainability, Cornell University, and the Link Foundation Energy Fellowship. C. N.'s effort was supported by the Cornell University Luis Stokes Alliance for Minority Participation (LSAMP) Program. We would also like to thank Ivan Keresztes, current director for the NMR facility at the Department of Chemistry and Chemical Biology, Cornell University for supporting our NMR experiments and analyses. Finally, we would like to thank Cord Heine, the environmental supervisor at Nucor Inc., in Auburn, NY for providing us with industrial residues used for this study.

References

1 S. J. Davis, N. S. Lewis, M. Shaner, S. Aggarwal, D. Arent, I. L. Azevedo, S. M. Benson, T. Bradley, J. Brouwer, Y. M. Chiang, C. T. M. Clack, A. Cohen, S. Doig, J. Edmonds, P. Fennell, C. B. Field, B. Hannegan, B. M. Hodge, M. I. Hoffert, E. Ingersoll, P. Jaramillo, K. S. Lackner, K. J. Mach, M. Mastrandrea, J. Ogden, P. F. Peterson, D. L. Sanchez, D. Sperling, J. Stagner, J. E. Trancik, C. J. Yang and K. Caldeira, *Science*, 2018, **360**(6396), eaas9793.

2 M. A. R. S. Koohi-fayegh, *Energy Ecol. Environ.*, 2016, **1**, 10–29.

3 M. A. Pellow, C. J. M. Emmott, C. J. Barnhart and S. M. Benson, *Energy Environ. Sci.*, 2015, **8**, 1938–1952.

4 L. Chen, Z. Qi, S. Zhang, J. Su and G. A. Somorjai, *Catalysts*, 2020, **10**, 858.

5 B. Parkinson, P. Balcombe, J. F. Speirs, A. D. Hawkes and K. Hellgardt, *Energy Environ. Sci.*, 2019, **12**, 19–40.

6 F. Eljack and M.-K. Kazi, *Front. Sustain.*, 2021, **1**, 1–15.

7 S. Zhang, Y. Liu, M. Zhang, Y. Ma, J. Hu and Y. Qu, *Nat. Commun.*, 2022, **13**, 5527.

8 P. D. Vaidya and J. A. Lopez-Sanchez, *ChemistrySelect*, 2017, **2**, 6563–6576.

9 T. M. C. Hoang, A. K. K. Vikla and K. Seshan, *Aqueous-phase reforming of sugar derivatives: Challenges and opportunities*, 2016, vol. 2016.

10 A. I. Osman, N. Mehta, A. M. Elgarahy, M. Hefny, A. Al-Hinai, A. H. Al-Muhtaseb and D. W. Rooney, *Hydrogen production, storage, utilisation and environmental impacts: a review*, Springer International Publishing, 2022, vol. 20.

11 G. Zoppi, G. Pipitone, R. Pirone and S. Bensaid, *Catal. Today*, 2022, **387**, 224–236.

12 J. Plácido and S. Capareda, *Bioresour. Bioprocess.*, 2016, **3**, 1–12.

13 U.S. Energy Information Administration, *Monthly Biodiesel Production Report*, 2015.

14 F. Yang, M. A. Hanna and R. Sun, *Biotechnol. Biofuels*, 2012, **5**, 1–10.

15 J. Moestedt, B. Müller, Y. Nagavara Nagaraj and A. Schnürer, *Front. Energy Res.*, 2020, **8**, 1–15.

16 T. Uekert, F. Dorchies, C. M. Pichler and E. Reisner, *Green Chem.*, 2020, **22**, 3262–3271.

17 I. Coronado, M. Stekrova, L. García Moreno, M. Reinikainen, P. Simell, R. Karinen and J. Lehtonen, *Biomass Bioenergy*, 2017, **106**, 29–37.

18 Z. Xiong, Z. Fang, L. Jiang, H. Han, L. He, K. Xu, J. Xu, S. Su, S. Hu, Y. Wang and J. Xiang, *Fuel*, 2022, **314**, 122746.

19 L. André, S. Abanades and G. Flamant, *Renewable Sustainable Energy Rev.*, 2016, **64**, 703–715.

20 D. A. Boga, F. Liu, P. C. A. Bruijnincx and B. M. Weckhuysen, *Catal. Sci. Technol.*, 2016, **6**, 134–143.

21 R. R. Davda and J. A. Dumesic, *Chem. Commun.*, 2004, 36–37.

22 M. Alvear, A. Aho, I. L. Simakova, H. Grénman, T. Salmi and D. Y. Murzin, *Catal. Sci. Technol.*, 2020, **10**, 5245–5255.

23 H. Xiong, A. DeLaRiva, Y. Wang and A. K. Datye, *Catal. Sci. Technol.*, 2015, **5**, 254–263.

24 T. Nozawa, Y. Mizukoshi, A. Yoshida and S. Naito, *Appl. Catal., B*, 2014, **146**, 221–226.

25 H. Harju, G. Pipitone and L. Lefferts, *Front. Chem.*, 2020, **8**, 1–13.

26 J. Zhang, W. Yan, Z. An, H. Song and J. He, *ACS Sustainable Chem. Eng.*, 2018, **6**, 7313–7324.

27 S. Jeon, H. S. Roh, D. J. Moon and J. W. Bae, *RSC Adv.*, 2016, **6**, 68433–68444.

28 P. Ochonma, C. Blaudeau, R. Krasnoff and G. Gadikota, *Front. Energy Res.*, 2021, **9**, 1–16.

29 F. Raganati, F. Miccio and P. Ammendola, *Energy Fuels*, 2021, **35**, 12845–12868.

30 T. Yin, S. Yin, A. Srivastava and G. Gadikota, *Resour., Conserv. Recycl.*, 2022, **180**, 106209.

31 S. Fujikawa, R. Selyanchyn and T. Kunitake, *Polym. J.*, 2021, **53**, 111–119.

32 S. Kodama, T. Nishimoto, N. Yamamoto, K. Yogo and K. Yamada, *Energy*, 2008, **33**, 776–784.

33 G. Gadikota, *Commun. Chem.*, 2021, **4**, 1–5.

34 M. Liu and G. Gadikota, *Fuel*, 2020, **275**, 1–37.

35 G. Gadikota, *Nat. Rev. Chem.*, 2020, **4**, 78–89.

36 G. Gadikota, J. Matter, P. Kelemen and A. H. A. Park, *Phys. Chem. Chem. Phys.*, 2014, **16**, 4679–4693.

37 V. Nikulshina, M. E. Gálvez and A. Steinfeld, *Chem. Eng. J.*, 2007, **129**, 75–83.

38 A. Stefánsson, P. Bénézeth and J. Schott, *Geochim. Cosmochim. Acta*, 2014, **138**, 21–31.

39 T. N. Borhani and M. Wang, *Renewable Sustainable Energy Rev.*, 2019, **114**, 109299.

40 J. W. Shabaker, G. W. Huber and J. A. Dumesic, *J. Catal.*, 2004, **222**, 180–191.

41 B. Roy and C. A. Leclerc, *J. Power Sources*, 2015, **299**, 114–124.

42 R. L. Manfro, T. P. M. D. Pires, N. F. P. Ribeiro and M. M. V. M. Souza, *Catal. Sci. Technol.*, 2013, **3**, 1278–1287.
43 R. Ragipani, S. Bhattacharya and A. K. Suresh, *React. Chem. Eng.*, 2021, **6**, 1152–1178.
44 B. Xu and Y. Yi, *Chemosphere*, 2022, **287**, 132274.
45 G. Gadikota and A. H. A. Park, *Accelerated Carbonation of Ca- and Mg-Bearing Minerals and Industrial Wastes Using CO2*, Elsevier B.V., 2015.
46 S. Y. Pan, T. C. Chung, C. C. Ho, C. J. Hou, Y. H. Chen and P. C. Chiang, *Sci. Rep.*, 2017, **7**, 1–11.
47 M. Fridahl and M. Lehtveer, *Energy Res. Soc. Sci.*, 2018, **42**, 155–165.
48 J. Rogelj, D. Shindell, K. Jiang, S. Fifita, P. Forster, V. Ginzburg, C. Handa, H. Kheshgi, S. Kobayashi and E. Kriegler, *Glob. Warm. 1.5° C*, 2018, pp. 93–174.
49 R. R. Davda, J. W. Shabaker, G. W. Huber, R. D. Cortright and J. A. Dumesic, *Appl. Catal., B*, 2005, **56**, 171–186.
50 J. De Heer, *J. Chem. Educ.*, 1957, **34**, 375–380.
51 A. Korchef and M. Touaibi, *Water Environ. J.*, 2020, **34**, 331–341.
52 G. Gravogl, F. Birkelbach, D. Müller, C. L. Lengauer, P. Weinberger and R. Miletich, *Adv. Sustainable Syst.*, 2021, **5**, 1–11.
53 Q. Qian, J. Zhang, M. Cui and B. Han, *Nat. Commun.*, 2016, **7**, 1–7.
54 D. Li, Y. Li, X. Liu, Y. Guo, C. W. Pao, J. L. Chen, Y. Hu and Y. Wang, *ACS Catal.*, 2019, **9**, 9671–9682.
55 N. D. Subramanian, J. Callison, C. R. A. Catlow, P. P. Wells and N. Dimitratos, *Int. J. Hydrogen Energy*, 2016, **41**, 18441–18450.
56 G. Pipitone, G. Zoppi, R. Pirone and S. Bensaid, *Int. J. Hydrogen Energy*, 2022, **47**, 151–180.
57 A. Patra, H. Peng, J. Sun and J. P. Perdew, *Phys. Rev. B*, 2019, **100**, 1–8.
58 C. Liu, K. Shih, Y. Gao, F. Li and L. Wei, *J. Soils Sediments*, 2012, **12**, 724–733.
59 J. Fermoso, L. He and D. Chen, *J. Chem. Technol. Biotechnol.*, 2012, **87**, 1367–1374.
60 D. J. M. De Vlieger, B. L. Mojet, L. Lefferts and K. Seshan, *J. Catal.*, 2012, **292**, 239–245.